Macromolecules

Article

pubs.acs.org/Macromolecules

Rational Design of Organotin Polyesters

Aaron F. Baldwin,[†] Tran Doan Huan,[‡] Rui Ma,[†] Arun Mannodi-Kanakkithodi,[‡] Mattewos Tefferi,[§] Nathan Katz,[†] Yang Cao,[§] Rampi Ramprasad,[‡] and Gregory A. Sotzing*[,†]

[†]Polymer Program, University of Connecticut, 97 North Eagleville Road, Storrs, Connecticut 06269, United States

[‡]Department of Materials Science and Engineering, University of Connecticut, 97 North Eagleville Road, Storrs, Connecticut 06269, United States

[§]Department of Electrical and Computer Engineering, University of Connecticut, 97 North Eagleville Road, Storrs, Connecticut 06269, United States

Supporting Information

ABSTRACT: Large dielectric constant and band gap are essential for insulating materials used in applications such as capacitors, transistors and photovoltaics. Of the most common polymers utilized for these applications, polyvinyldiene fluoride (PVDF) offers a good balance between dielectric constant, >10, and band gap, 6 eV, but suffers from being a ferroelectric material. Herein, we investigate a series of aliphatic organotin polymers, p[DMT-$(CH_2)_n$], to increase the dipolar and ionic part of the dielectric constant while maintaining a large band gap. We model these polymers by performing first-principles calculations based on density functional theory (DFT), to predict their structures, electronic and total dielectric constants and energy band gaps. The modeling and experimental values show strong correlation, in which the polymers exhibit both high dielectric constant, ≥5.3, and large band gap, ≥4.7 eV with one polymer displaying a dielectric constant of 6.6 and band gap of 6.7 eV. From our work, we can identify the ideal amount of tin loading within a polymer chain to optimize the material for specific applications. We also suggest that the recently developed modeling methods based on DFT are efficient in studying and designing new generations of polymeric dielectric materials.

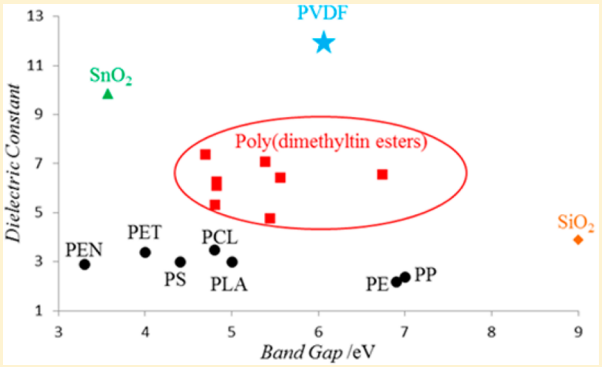

1. INTRODUCTION

Upon application of an electric field, a dielectric/insulating material will polarize causing a shift in charges from equilibrium without electrical conduction. As a result of this phenomenon, these types of materials have found widespread use in numerous applications such as capacitors, field effect transistors (FETs), electromechanical systems, and photovoltaics.[1−4] The demand for new materials expands exponentially as the development of these applications continues to grow with new devices coming to fruition including railguns, electromagnetic aircraft launch system (EMALS) and hybrid electric vehicles for instance.[5−7] Therefore, much research has been devoted to developing higher dielectric constant materials in order to achieve lightweight device miniaturization.

Compared to ordinary dielectric ceramics, polymers meet the lightweight requirement with easier processing, but suffer from either having a low dielectric constant or band gap, Figure 1. To increase the dielectric constant of insulating films two methods have become popular: (1) incorporation of a larger permanent dipole moment within the polymer backbone to increase orientational polarization, with polyvinyldiene fluoride (PVDF) being one of the most studied polymers since it also has a large band gap, ca. 6 eV, or (2) the addition of high dielectric constant inorganic nanoparticles fillers to introduce interfacial polarization between particle and polymer.[8] However, both of these methods have some limitations. Though PVDF has a dielectric constant >10, it is ferroelectric in nature and suffers from large dielectric losses while nanocomposite films may require large volumes of nanoparticles to achieve an increase of the dielectric constant and as a consequence may reduce the dielectric breakdown field.[9]

Herein, based on first-principles calculations performed at the DFT level, we investigate the effect of the amount of tin loading within the polymer backbone, by varying the length of the aliphatic diacid segment, on properties such as low-energy structural motifs, dielectric constants, dielectric loss and energy band gap. One of our conclusions is that aliphatic poly(organotin esters), denoted as p[DMT$(CH_2)_n$], are promising polymeric dielectric materials. Furthermore, the agreement between calculated and measured data suggests that the simulation strategy used in our work is useful and effective in designing advanced dielectric materials.

Received: December 1, 2014
Revised: April 3, 2015

DOI: 10.1021/ma502424r
Macromolecules XXXX, XXX, XXX−XXX

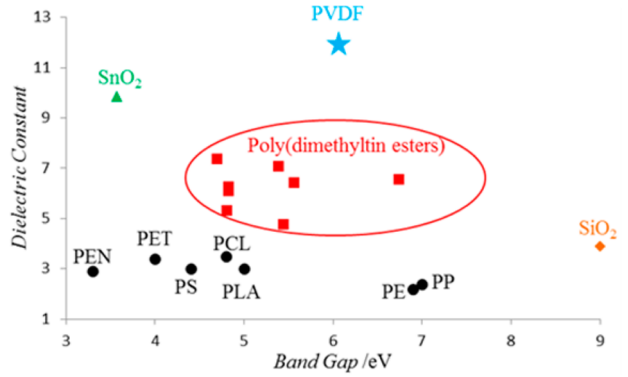

Figure 1. Dielectric constant versus band gap of poly(dimethyltin esters) (red squares), polyvinylidene fluoride (PVDF) (blue star), linear dielectric polymers polypropylene (PP), low density polyethylene (PE), polylactide (PLA), polycaprolactone (PCL), polystyrene (PS), polyethylene terephthalate (PET) and polyethylene naphthalate (PEN) (black circles), SiO_2 (orange diamond), and SnO_2 (green triangle). The data for the common polymers was obtained from ref 8i.

2. THEORETICAL AND EXPERIMENTAL METHODS

2.1. Theoretical Methods. The computational workhorse used in this study is density functional theory (DFT) as implemented in the Vienna ab initio simulation package (VASP).[10−12] The total energies, E_{DFT}, of the examined structural models were calculated with the Perdew−Burke−Ernzerhof (PBE) exchange-correlation (XC) functional.[13] For tin, carbon, oxygen, and hydrogen, the $4d^{10}5s^25p^2$, $2s^22p^2$, $2s^22p^4$, and $1s^1$ states were treated as the valence states. Monkhorst−Pack *k*-point meshes with spacing of 0.1 $Å^{-1}$ are used for integrations over the Brillouin zones of the models.[14] A plane wave kinetic energy cutoff is chosen to be 500 eV while atomic and cell variables were simultaneously relaxed until the residual forces were smaller than 10^{-2} eV $Å^{-1}$.

DFT calculations are essentially based on first-principles, making them versatile, but computationally expensive. Even though polymers, in general, display complex morphologies, they are usually modeled as ideal crystals or infinite single chains at the DFT level.[15−18] Such a simplified approach seems to be powerful in capturing several of the properties of our interest, e.g., energy band gap and dielectric constant.[10,15,19−21] In this work, we modeled p[DMT$(CH_2)_n$] as ideal, three-dimensional crystalline materials.

Still, predicting even the simplest crystalline structures of a new polymeric system is a challenge, in and of itself. Here, the possible stable structures of p[DMT$(CH_2)_n$] were predicted using the minima-hopping method which is able to explore the low-energy regions of the corresponding configurational space.[22−24] Because this method employs no constraint, unknown structural motifs may readily be predicted from any initial structure. The reliability of this method has been shown in a number of structure prediction works.[25] To start the prediction process, the initial structures assumed for p[DMT$(CH_2)_n$], as shown in Scheme 1, were manually designed by assembling two methyl (CH_3) groups and two carboxyl (C(=O)O) groups with a tin atom. A chain of nCH_2 groups was then added to link the obtained dimethyltin dicarboxylate groups. From these starting points, different low-energy structures of p[DMT$(CH_2)]_n$ can readily be predicted with the minima-hopping method.

Once the most stable structures of p[DMT$(CH_2)_n$] were predicted, the dielectric constants were then calculated within the density functional perturbation theory as implemented in VASP code.[26] Because PBE is well documented to systematically underestimate E_g, this quantity was also calculated with the Heyd−Scuseria−Ernzerhof (HSE06) XC hybrid functional.[27,28] Following previous computational works,[22−25] the intermolecular van der Waals interactions, which play an essential role in stabilizing polymers, were estimated by DFT-D2, the method proposed by Grimme.[29]

Scheme 1. Synthetic Procedure for the Preparation of Aliphatic Poly(dimethyltin esters) (Top), Where Polymers Can Be Pressed into Pellets or Solution Casted into Films (Bottom)

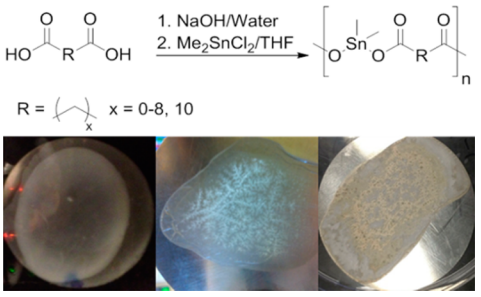

2.2. Materials and Synthetic Procedure. All diacids, 1,2-dichloroethane (1,2-DCE) and *m*-cresol were procured from Acros Organics. Succinic acid was purchased as the disodium salt form and oxalic acid was the dihydrate form from Acros Organics. Dimethyltin dichloride was procured from TCI America. Sodium hydroxide (NaOH) and triethylamine (TEA) were purchased from Fisher Scientfic. All monomers were used as received. Tetrahydrofuran (HPLC grade) was purchased from J.T. Baker. 1,1,1,3,3,3-hexafluoroisopropanol (HFIP) was procured from Synquest Laboratories and chloroform was purchased from BrandNu. Deionized water was obtained using a Millipore purification system. Stainless steel shim stocks (diameter = 2 in., thickness = 0.01 in., and ASTM A666 stainless steel) were acquired from McMaster Carr. Quartz glass slides (3 in. × 1 in. × 1 mm) were procured from Ted Pella, Inc.

In general, Scheme 1; a molar excess of the diacid was added to a round bottomed flask and dissolved in 20 mL of water. To the diacid solution was added 2.1 equiv, with respect to the diacid, of sodium hydroxide. To the rapidly stirred aqueous solution was added 20 mL of a dimethyltin dichloride solution in tetrahydrofuran. The precipitate is filtered and washed with 50 mL portions of tetrahydrofuran and water and dried *in vacuo* at 115 °C for 20 h to remove any residual solvent (see Supporting Information for full details of syntheses and characterization).

3. STRUCTURAL MOTIFS AND CHARACTERIZATION

It has been reported that the coordination number of a tin atom in organotin compounds can be four, five, six, or seven.[30] In the low-energy structures predicted for p[DMT$(CH_2)_n$], the central tin atom of each dimethyltin dicarboxylate group are coordinated by six atoms, including two carbon atoms from two methyl groups and four oxygen atoms from the surrounding carboxyl groups. On the basis of the arrangement of the four Sn−O bonds, the predicted structures are categorized into three structural motifs, α, β, and γ, which are illustrated in Figure 2.

Motifs α and β (also called intrachain and interchain) were previously hypothesized to exist in organotin compounds.[31] In motif α (intrachain), the two carboxyl groups from the same repeat unit are bonded to the central tin atom by four Sn−O bonds, two of them are rather long (≥2.5 Å) and weak while the other two are short and strong (≈2.1 Å). Consequently, motif α is characterized by one-dimensional chains held together by the long-range dispersion interactions. In a number of organotin compounds, e.g., organotin carboxylates, dibutanidobis(2,4,6-trimethylbenzoato)tin, and di-*n*-butyl-(glutarato)tin(IV), this motif has been reported.[32−34] A quantitative examination reveals that the characteristic bond lengths and bond angles predicted for p[DMT$(CH_2)_n$] (specifically for p(DMTGlu) agree very well with those

DOI: 10.1021/ma502424r
Macromolecules XXXX, XXX, XXX−XXX

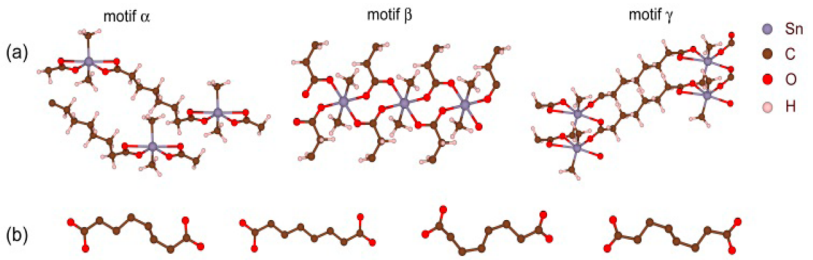

Figure 2. (a) Lowest-energy structures of α (intrachain), β (interchain) and γ (hybrid) motifs predicted for p(DMTSub) and (b) four (out of numerous) folding geometries of the chains of methylene groups acting as organic linkers in p(DMTSub). In the figure, tin atoms (gray spheres) are 6-fold coordinated by four oxygen atoms (red spheres) from ester groups and two carbon atoms (dark-brown) from two methyl groups. Hydrogen atoms are shown as pink spheres.

measured in the related compounds.[32,33] In the so-called motif β (interchain), four Sn−O bonds link the central tin atom with four different carboxyl groups, two of them belonging to the same chain (repeat unit) while the other two bonds come from other chains. Therefore, motif β is characterized by patterns of two-dimensional layers. In many cases (based on the value of n), motif β features the most stable structure predicted. A new motif, called γ, was also predicted, combining the essential characteristics of motifs α and β. As shown in Figure 2a, two Sn−O bonds are shared with the carboxyl group from the same repeat unit while the other two Sn−O bonds link the central tin atom with two carboxyl groups from other chains.

For each member of the polymer family examined, many low-energy structures of the same motif were predicted, differing only by the folding geometry of the methylene chains (see Figure 2b for an illustration). The energetic information obtained for the most stable structures of each motif indicates that these motifs are slightly different by a few millielectronvolts per atom (see Supporting Information for a graphical illustration). For each motif, the number of folding geometries of the methylene chains increases dramatically with the linker length, n, generating an associated "energy spectrum". Because these spectra heavily overlap, it is suggested that all of these motifs may easily coexist in the experimental samples under ambient conditions.

To confirm the presence of these motifs within the polymers, IR and XRD were performed. Within IR, the formation of the tin carboxylate bond is marked by the presence of five absorptions: a combination skeletal C−CO−O− coupled with Sn−O stretching and both asymmetric and symmetric bridging and nonbridging carbonyl stretches.[35] All of the polymers have an IR absorption peak in the range of 610−656 cm^{-1} indicative of the skeletal stretching. The asymmetric and symmetric bridging and nonbridging carbonyl stretches are characteristic of the formation of the octahedral coordination complexes. As stated before, Peruzzo et al. hypothesized that both inter- and intrachain complexes could be present, while Carraher labeled the asymmetric nonbridging and bridging at 1635−1660 cm^{-1} and 1550−1580 cm^{-1}, respectively and the symmetric bridging and nonbridging at 1410−1430 cm^{-1} and 1350−1370 cm^{-1}, respectively.[31,35] Figure 3 depicts the region in the IR spectra in which the coordination complexes of the aliphatic poly(dimethyltin esters) are observed (see Supporting Information for individual IR spectra for all polymers). As illustrated in Figure 3 all four of the absorptions are present in varying intensities which is due to the presence of the three different motifs. The intensity of the symmetric bridging and nonbridging carbonyl absorption is approximately equal with the exception of p(DMTSuc) which exhibits a much stronger peak for the nonbridging than bridging. Since, the α motif (intrachain) of p(DMTSuc) theoretically does not form then the nonbridging stretches should be reduced in intensity, but this is not the case. Therefore, the p(DMTSuc) must favor a hybrid type structure that has more intrachain coordination versus interchain coordination (see Supporting Information for IR spectra).

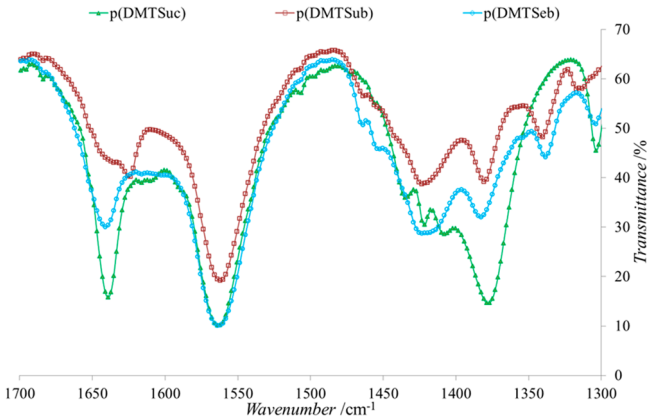

Figure 3. FT-IR of poly(dimethyltin succinate) (closed green triangles), poly(dimethyltin suberate) (open brown rectangles), and poly(dimethyltin sebacate) (open blue diamonds).

As a compliment to IR, X-ray diffraction (XRD) was performed on the polymer powders to verify that the structure of these polymers are quite complex. The XRD patterns, illustrated in Figure 4, show that the structure of the polymers are not exact representations of the α, β, and γ motifs, but a conglomeration of each of these motifs in some unknown ratio within the polymer chain. Though only two XRD patterns are shown in Figure 4, this observation holds true for all of the aliphatic poly(organotin esters) (see Supporting Information for XRDs of all polymers).

4. DIELECTRIC PROPERTIES

The static dielectric constant, ε, is an essentially important factor in the performance of a dielectric for any application. Generally, ε is a second rank tensor quantity, describing the response of an insulator to the external electric field in the linear regime. There are two contributions to ε, an electronic dielectric constant tensor ε_{el} related to the refractive index of the material and an ionic dielectric constant tensor ε_{ion}.[19,36,37] Given that at the macroscopic scales, polymers are not precisely ideal crystals and become isotropic, ε and its contributions can

DOI: 10.1021/ma502424r
Macromolecules XXXX, XXX, XXX−XXX

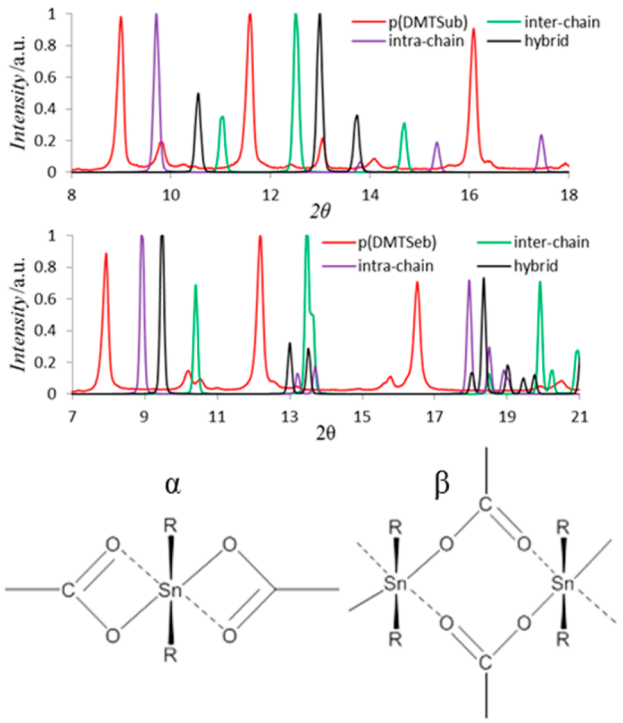

Figure 4. Experimental XRD of poly(dimethyltin suberate) and poly(dimethyl sebacate) with predicted diffraction patterns of the intrachain (α), interchain (β), and hybrid (γ) motifs.

naturally be reported as a scalar quantity represented by the trace of the respective tensors.

Theoretically, ε of the most stable structures of the motifs predicted for p[DMT$(CH_2)_n$] is shown in Figure 4A to be heavily motif dependent. Overall, the general trend is that ε decreases as n becomes large. Up to n = 11, ε of the examined polymers is as high as 4.0, roughly 50% higher than $\varepsilon \approx 2.6$, calculated for PE. The dependence of ε on n mostly originates from εion because $\varepsilon_{el} \approx 2.7-3.0$ for all of the examined values of n.

We further analyzed the motif dependence of ε_{ion}. A typical example for this strong dependence is the case of p(DMTPim), of which ε_{ion} is calculated to be 1.74 and 3.44 for motifs α and β, respectively. To clarify this large difference, we determined the vibration mode that most significantly contributes to εion of each motif (see Supporting Information for illustrative representation). For α, all four highly polarized Sn−O bonds are in bending vibrations while for β, two of these bonds are clearly in their stretching modes. It is worth noting here that because of the two-dimensional nature of motif β, the orientations of the four Sn−O bonds are "more isotropic" than motif α, thus stretching vibrations are more likely to occur. Because these stretching vibrations generally lead to larger changes in the Sn−O bond length, one may qualitatively expect that motif β is highly polarizable with higher ε_{ion}.

As a result of the insolubiltiy of some of the poly(dimethyltin esters), pellets were pressed in order to compare the theoretical calculations to experimental dielectric values as well as the effect of increasing the methylene spacer between the dimethyltin dicarboxylate functional group on these values. The aliphatic poly(dimethyltin esters) represent polymers that have 33% functionality, p(DMTDec) to 100% functionality, p(DMTOx), in the polymer backbone. Figure 5 represents the

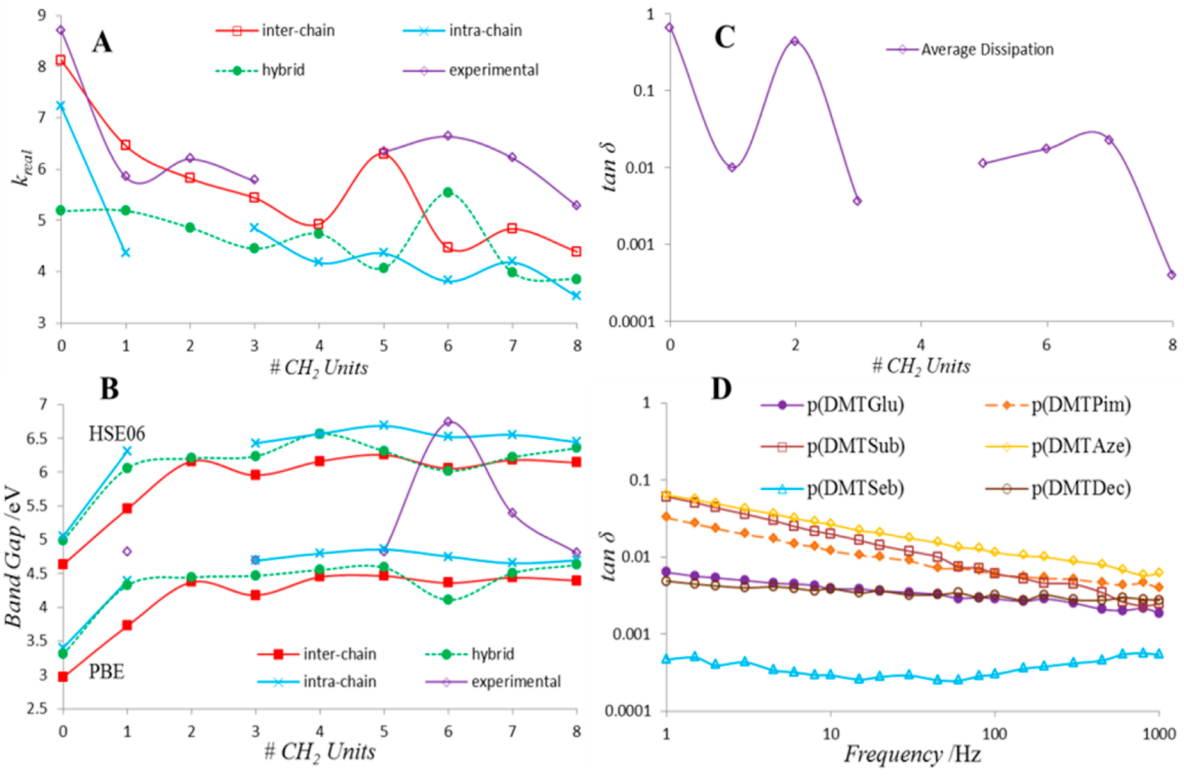

Figure 5. Theoretical and experimental values of dielectric constant (A) and band gap (B) of poly(dimethyltin esters). Averaged (1−1000 Hz) experimental dissipation factor (C) for poly(dimethyltin esters) and experimental dissipation factor of poly(dimethyltin esters) with no. of CH_2 units = 3,5−8,10 (D).

DOI: 10.1021/ma502424r
Macromolecules XXXX, XXX, XXX−XXX

dielectric properties of the poly(dimethyltin esters) versus the theoretical calculations. Averaging the dielectric constant, εavg, from 1 to 1000 Hz, Figure 4A, also illustrates that the dielectric constant follows the odd/even property rule commonly found in polymers. Comparing ε_{avg} to the theoretical calculations shows that the experimental values are within 44% versus the average value of the three motifs. As seen in Figure 4 the experimental dielectric constant is closer to the intra chain motif with the exception of p(DMTSub), and thus comparing these values the difference is within 29% with the best relation being p(DMTPim) which is 0.6%. The difference in the theoretical and experimental values can be attributed to the DFT calculations being performed on systems on fully crystalline materials at 0 K. What is more intriguing is that as the number of methylene units is increased from 0 to 3 there is a decrease in the dielectric constant and then there is a spike in the dielectric constant to a second maxima at six methylene groups. This trend in dielectric constant is accurately predicted by the DFT calculations which show the spike at either five methylene groups for the α and β motifs or six for the γ structure. The maxima at six methylene groups is expected since the polymer chains take a hybrid motif as seen by IR and XRD. The dielectric constant of the aliphatic poly(dimethyltin esters) reaches a minimum of 5.3 for both p(DMTSeb) and p(DMTDec).

Insulator performance is not only influenced by the dielectric constant but also the dielectric loss. P(DMTOx) and p(DMTSuc), Figure 4C, suffer from the highest losses as a result of increased DC conductivity within the sample at lower frequencies which in the case of p(DMTOx) could be attributed to residual water even after extensive drying of the pellet in vacuo (see Supporting Information for TGAs). The loss factor of the majority of the aliphatic polymers are on the order of 10^{-2} which, in comparison with PE and PP, is on the same order of magnitude, Figure 5D. P(DMTSeb) is the only aliphatic polymer that has a dissipation factor on the order of insulating polymers used in pulsed power systems ($\sim 10^{-4}$). The expected trend in loss should be a decrease as the number of methylene groups is increased due to the polymer becoming more like poly(ethylene) with a decrease in dipole moment density in the backbone. However, these polymers do not exhibit this trend and the loss of these polymers is roughly on the same order of magnitude.

5. ENERGY BAND GAPS

High breakdown strength is desirable for an ideal dielectric material, allowing it to work under high voltages and increasing its energy density. This quantity is however not easy to compute. In recent work, a model for estimating the upper bound of the breakdown strength of a material was developed and applied to a variety of model insulators.[38] The predicted breakdown strength was shown to correlate well with the band gap, in that insulators with low (high) band gap values also display low (high) breakdown fields. Hence, in the present work, we view the band gap as a proxy for the breakdown strength.

It is a standard fact that E_g is usually underestimated by conventional DFT calculations with the PBE XC functional.[39] For highly crystalline PE, we obtained $E_g \approx 6.8$ eV using PBE, which is considerably smaller than the experimental value of 8.8 eV.[40] Using the HSE06 hybrid functional for the XC energies is much more computationally expensive but is also commonly known to be a better option for estimating E_g. With this functional, our calculated band gap is clearly improved to be $E_g \approx 8.4$ eV. In this work, we will not rule out PBE results in our discussion because both approaches include approximations that are hard to control.[39] The evolution of E_g as n increases is further examined by the density of states calculated at the HSE06 level for the lowest energy structures of motif β, noting that E_g is insensitive to which motif the polymer takes. As shown in Figure 6, states related to the dimethyltin

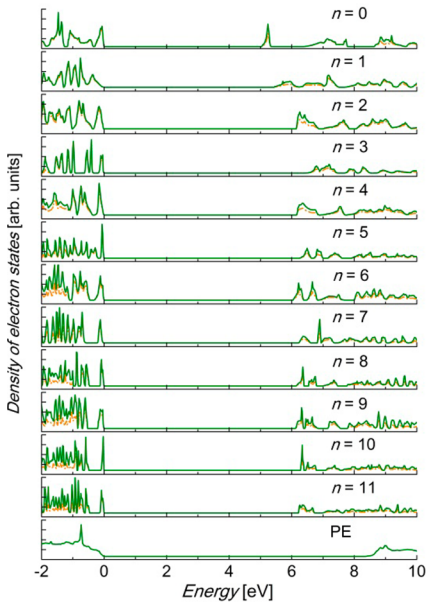

Figure 6. Electron density of states calculated for the predicted most stable structures of p[DMT$(CH_2)_n$], shown by solid dark-green curves. Contribution from tin and its six coordinated (two carbon and four oxygen) atoms are shown by orange curves. Fermi energies are set to zero.

dicarboxylate groups dominate the valence band maximum and the conduction band minimum, limiting the E_g to about 6.0 eV. It may be expected that in the limit of $n \rightarrow \infty$, the significance of these states will be diminished and the calculated band gap may approach the band gap of crystalline PE.

In order to determine whether this trend is true, films of the poly(dimethyltin esters) were casted from *m*-cresol solutions, with the exception of p(DMTMal) and p(DMTSub) which were casted from 3:1 (v:v) HFIP:CHCl3 and 2:1 (v:v) *m*-cresol:1,2-DCE respectively, onto quartz glass slides and measured using UV−vis. The E_g was then calculated from Planck's relation after determining the onset wavelength of abosrption (λ_{onset}). The shoulder peak adjacent to the edge of the onset observed in some polymers is presumed to be localized electronic states lying above the valence band or below the conduction band and is seen in other polymers such as PE or PP (see Supporting Information for UV−vis spectra).[8i] Figure 5B illustrates the experimental polymer band gaps versus the calculated results. The experimental band gaps of the aliphatic poly(dimethyltin esters) range from 4.7 to 6.7 eV, which could be indicative of a high breakdown potential for this system of polymers. Compared to the calculated band gaps, the measured band gaps of the polymers were within 25% of the averaged calculated band gap for the intrachain, interchain and hybrid motifs for each polymer for both PBE and HSE06 functionals, with the only outlier being p(DMTSub) versus the PBE result. Given that ε and E_g evolve oppositely as n increases,

DOI: 10.1021/ma502424r
Macromolecules XXXX, XXX, XXX−XXX

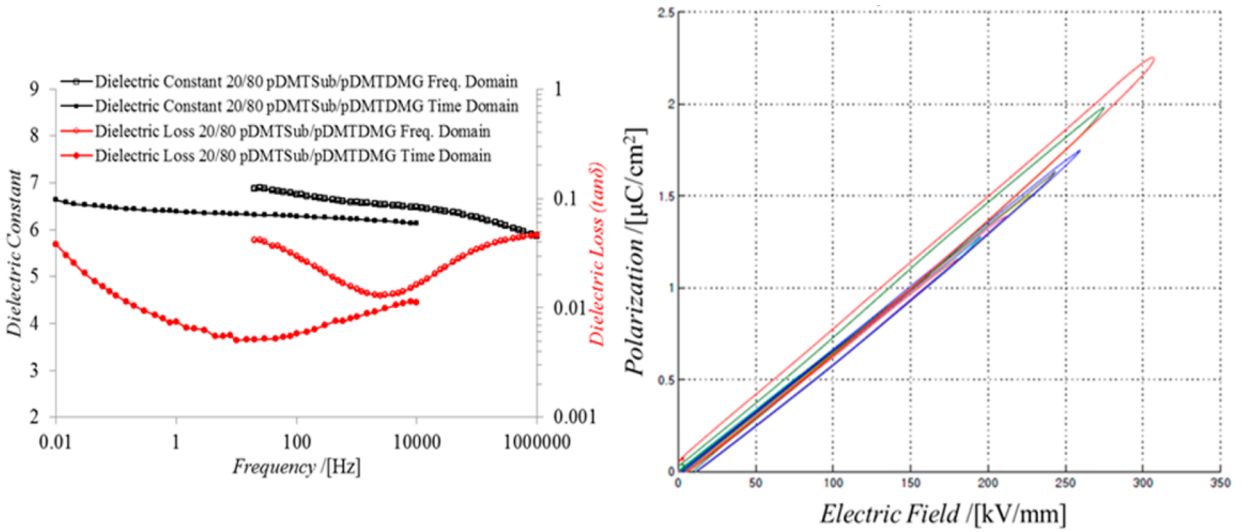

Figure 7. Frequency and time domain dielectric properties (left) and polarization vs electric field loops (right) for the 20/80 (w/w) blend of p(DMTSub)/(pDMTDMG), suggesting linear polarizations for electric fields up to 300 kV cm^{-1}. Dielectric permittivity derived from the DE loops is in agreement with frequency domain data over the range of 10^{-2}–10^{6}Hz.

n = 5–8 can be identified as the optimal length of the methylene linker segment in which the energy density of the polymer may be maximized. Of course, as mentioned previously, the breakdown field strengths of these materials have to be determined for this conclusion to be completely appropriate.

6. ELECTRICAL BREAKDOWN MEASUREMENTS

The shortcoming of the aliphatic poly(dimethyltin esters) is that they form large crystals upon drying, in which the size of the crystal is dependent upon the length of the methylene linker. Previously,[41] we have blended a second organotin ester, poly(dimethyltin 3,3-dimethylglutarate) (p(DMTDMG)), whereupon the two pendant methyl groups attached to the diacid have given rise to sufficient chain disruption leading to very small crystal size and better adhesion to the stainless steel shim stock. This experiment was repeated by blending p(DMTSub) with p(DMTDMG), as p(DMTSub) exhibited the highest dielectric constant and band gap of the soluble aliphatic poly(dimethyltin esters). Films were drop cast from a 5 wt % solution of 20/80 (wt:wt) p(DMTSub)/p(DMTDMG) in *m*-cresol onto shim stocks. The films were then heated on a hot plate to drive off *m*-cresol and once the films were tacky they were further dried in vacuo at 130 °C for 24 h. The film thickness was then measured using a point-to-point thickness gauge (model LE1000-2, MeasureItAll) at five places and subtracting the thickness of the shim stock. Since this measurement involves determining a small number from difference of two large numbers, the film thickness was independently measured by coating a thick layer of gold on top of the film and cutting a cross section with a focused ion beam (FIB). The layers are then identified and the thickness determined. These numbers agree well, respectively. Mechanical profilometry was also performed to determine sample roughness, which showed variation in thickness ranging between 0.0096 and 0.0135 μm, 0.064–0.09% based on the 15 μm sample.

The charge–discharge of the 20/80 p(DMTSub)/p(DMTDMG) blend was then determined through measurement of D–E hysteresis loops and is depicted in Figure 7. The maximum breakdown field achieved was ca. 300 kV mm^{-1}, which resulted in an energy density of ca. 4 J cm^{-3} and a corresponding efficiency of 90% (see Supporting Information for plots). On the basis of the hysteresis loop, the loss at high field is due to conduction rather than remnant polarization. A comparison of the dielectric constant measured in the frequency and time domain versus the D–E loop shows correlation, 6.4 and 6.5, respectively, though at an electric field above 300 mV m^{-1}, the dielectric constant increases to slightly above 7. The difference in the two values can be attributed to the size of the electrode in which the measurements are taken, 0.78 and 0.07 cm^2 for the frequency/time domain and D–E loop, respectively.

7. CONCLUSION

In summary, we have presented a thorough modeling and experimental study on aliphatic poly(dimethyltin esters), a family of polymers that may be used in a variety of applications which require the use of dielectric materials. This work has employed several state-of-the-art methods at the level of density functional theory to predict and study the polymeric materials of interest. The structural models proposed for p[DMT-$(CH_2)_n$] display a high level of agreement with the experimental values which show that this series of polymers exhibit high dielectric constant, $\varepsilon \geq 5.3$, with low dielectric loss for some polymers, $\leq 10^{-2}$, and large band gaps, $E_g \geq 4.6$ eV. On the basis of these results we can identify some value of the methylene chain length n at which the polymeric material can be optimized in terms of the desired application. Further studies, such as processing conditions to create large uniform films in which morphology is controlled, will also be performed on the blend to increase the breakdown field. This work also indicates that the strategies used to study p[DMT$(CH_2)_n$] are technically feasible and can be further used in investigating these tin motifs as well as other material design problems.

■ ASSOCIATED CONTENT

Supporting Information

Experimental and characterization data. This material is available free of charge via the Internet at http://pubs.acs.org.

DOI: 10.1021/ma502424r
Macromolecules XXXX, XXX, XXX–XXX

AUTHOR INFORMATION

Corresponding Author

*(G.A.S.) E-mail: sotzing@mail.ims.uconn.edu.

Author Contributions

A.F.B. and T.D.H. contributed equally in the preparation of this work.

Notes

The authors declare no competing financial interest.

ACKNOWLEDGMENTS

This work was supported by a Multi-University Research Initiative (MURI) grant from the Office of Naval Research, under Award Number N00014-10-0944. The authors thank Max Amsler and Stefan Goedecker for making the minima-hopping code available. The authors also thank JoAnne Ronzello for performing the TDDS measurements. Computational work was made possible through the XSEDE computational resource allocation number TG-DMR080058N.

REFERENCES

(1) (a) Hergenrother, P. M. *High Perform. Polym.* **2003**, *15*, 3−45. (b) Thakur, V. K.; Kessler, M. R. In *Advance Energy Materials*; Tiwari, A., Valyukh, S., Eds., Scrivener Publishing: Beverly, MA, 2014; Vol. *1*, Ch. 5.

(2) (a) Ha, Y.-G.; Everaerts, K.; Hersam, M. C.; Marks, T. J. *Acc. Chem. Res.* **2015**, *47*, 1019−1028. (b) Diekmann, T.; Hilleringmann, U. In *Physical and Chemical Aspects of Organic Electronics*; Wöll, C., Ed.; Wiley-VCH: Weinheim, Germany, 2009; Vol. *1*, Ch. 18.

(3) Rebeiz, G. M. *RF MEMS: Theory, Design, and Technology*; Wiley: Hoboken, NJ, 2003.

(4) Camaioni, N.; Po, R. *J. Phys. Chem. Lett,*. **2013**, *4*, 1821−1828.

(5) Doyle, M. R.; Samuel, D. J.; Conway, T.; Klimowski, R. R. *IEEE Trans. Magn.* **1995**, *31*, 528−533.

(6) Clayton, D. H.; Sudhoff, S. D.; Grater, G. F. *Power Modulator Symp. (Norfolk, VA)* **2000**, 85−88.

(7) Beach, F.; McNab, I. *IEEE Conf. Pulsed Power* **2005**, 1−7.

(8) (a) Chung, T. C. M. *Macromolecules* **2013**, *46*, 6671−6698. (b) Chung, T. C. M. *Green Sustainable Chem.* **2012**, *2*, 29−37. (c) Yan, X. Z.; Goodson, T. *J. Phys. Chem. B* **2006**, *110*, 14667−14672. (d) Baldwin, A. F.; Ma, R.; Wang, C. C.; Ramprasad, R.; Sotzing, G. A. *J. Appl. Polym. Sci.* **2013**, *130*, 1276−1280. (e) Wang, Q.; Zhu, L. *J. Polym. Sci., B: Polym. Phys.* **2011**, *49*, 1421−1429. (f) Pan, J.; Li, K.; Chuayprakong, S.; Hsu, T.; Wang, Q. *ACS Appl. Mater. Interfaces* **2010**, *2*, 1286−1289. (g) Zhao, H.; Li, R. K. Y. *Composites: Part A* **2008**, *39*, 602−611. (h) Duan, C.−G.; Mei, W. N.; Hardy, J. R.; Ducharme, S.; Choi, J.; Dowben, P. A. *Europhys. Lett.* **2003**, *61*, 81−87. (i) Ohki, Y.; Fuse, N.; Arai, T. *2010 Annual Report Conference on Electrical Insulation and Dielectric Phenomena (West Lafayette, IN)* 2005; pp 1−4. (j) Ma, R.; Baldwin, A. F.; Wang, C. C.; Offenbach, I.; Cakmak, M.; Ramprasad, R.; Sotzing, G. A. *ACS Appl. Mater. Interfaces* **2014**, *6*, 10443−10451. (k) Sharma, V.; Wang, C. C.; Lorenzini, R. G.; Ma, R.; Zhu, Q.; Sinkovits, D. W.; Pilania, G.; Oganov, A. R.; Kumar, S.; Sotzing, G. A.; Boggs, S. A.; Ramprasad, R. *Nature Commun.* **2014**, DOI: 10.1038/ncomms5845.

(9) (a) Chu, B.; Zhou, X.; Ren, K.; Neese, B.; Lin, M.; Wang, Q.; Bauer, F.; Zhang, Q. M. *Science* **2006**, *313*, 334−336. (b) Guan, F.; Pan, J.; Wang, J.; Wang, Q.; Zhu, L. *Macromolecules* **2010**, *43*, 384−392. (c) Frost, N. E.; McGrath, P. B.; Burns, C. W. *IEEE Int. Symp. Electrical Insul.* **1996**, 300−303. (d) Nagao, D.; Kinoshita, T.; Watanabe, A.; Konno, M. *Polym. Int.* **2011**, *60*, 1180−1184.

(10) Kresse, G.; Furthmüller, J. *Comput. Mater. Sci.* **1996**, *6*, 15−50.

(11) Kresse, G. Ph. D. Thesis, Technische Universität Wien: Vienna, December, 1993.

(12) Kresse, G.; Furthmüller, J. *Phys. Rev. B* **1996**, *54*, 11169−11186.

(13) Perdew, J. P.; Burke, K.; Ernzerhof, M. *Phys. Rev. Lett.* **1996**, *77*, 3865−3868.

(14) Monkhorst, H. J.; Pack, J. D. *Phys. Rev. B* **1976**, *13*, 5188−5192.

(15) Zhu, Q.; Sharma, V.; Oganov, A. R.; Ramprasad, R. *J. Chem. Phys.* **2014**, *141*, 154102/1−154102/10.

(16) Bealing, C. R.; Ramprasad, R. *J. Chem. Phys.* **2013**, *139*, 174904.

(17) Pilania, G.; Wang, C. C.; Wu, K.; Sukumar, N.; Breneman, C.; Sotzing, G. A.; Ramprasad, R. *J. Chem. Inf. Model.* **2013**, *53*, 879−886.

(18) Pilania, G.; Wang, C. C.; Jiang, X.; Rajasekaran, S.; Ramprasad, R. *Sci. Rep.* **2013**, *3*, 2810/1−6.

(19) Wang, C. C.; Pilania, G.; Boggs, S. A.; Kumar, S.; Breneman, C.; Ramprasad, R. *Polymer* **2014**, *55*, 979−988.

(20) Gedde, U.; Mattozzi, A. *Long Term Properties of Polyolefins*; Springer: Berlin, 2004; Vol. *169*, pp 29−74.

(21) Furukawa, T.; Sato, H.; Kita, Y.; Matsukawa, K.; Yamaguchi, H.; Ochiai, S.; Siesler, H. W.; Ozaki, Y. *Polym. J.* **2006**, *38*, 1127−1136.

(22) Goedecker, S. *J. Chem. Phys.* **2004**, *120*, 9911−9917.

(23) Goedecker, S. *Modern Methods of Crystal Structure Prediction*; Oganov, A. R., Ed.; Wiley-VCH: Weinheim, Germany, 2011; Ch. 7, pp 147−180.

(24) Amsler, M.; Goedecker, S. *J. Chem. Phys.* **2010**, *133*, 224104−224111.

(25) (a) Huan, T. D.; Amsler, M.; Marques, M. A. L.; Botti, S.; Willand, A.; Goedecker, S. *Phys. Rev. Lett.* **2013**, *110*, 135502. (b) Huan, T. D.; Amsler, M.; Sabatini, R.; Tuoc, V. N.; Le, N. B.; Woods, L. M.; Marzari, N.; Goedecker, S. *Phys. Rev. B* **2013**, *88*, 024108.

(26) Baroni, S.; De Gironcoli, S.; Dal Corso, A. *Rev. Mod. Phys.* **2001**, *73*, 515−562.

(27) Heyd, J.; Scuseria, G. E.; Ernzerhof, M. *J. Chem. Phys.* **2006**, *124*, 219906.

(28) Krukau, A. V.; Vydrov, O. A.; Izmaylov, A. F.; Scuseria, G. E. *J. Chem. Phys.* **2006**, *125*, 224106/1−5.

(29) Grimme, S. *J. Comput. Chem.* **2006**, *27*, 1787−1799.

(30) Carraher, C. E. *Macromolecules Containing Metal and Metal-Like Elements: Group IVA Polymers*; Abd-El-Aziz, A. S., Carraher, C. E., Pittman, C. U., Zeldin, M., Eds.; Wiley: Hoboken, NJ, 2005; Vol. *4*, Ch. 10.

(31) (a) Plazzogna, G.; Peruzzo, V.; Tagliavini, G. *J. Organomet. Chem.* **1969**, *16*, 500−502. (b) Peruzzo, V.; Plazzogna, G.; Tagliavini, G. *Organomet. Chem.* **1969**, *18*, 89−94. (c) Peruzzo, V.; Plazzogna, G.; Tagliavini, G. *Organomet. Chem.* **1970**, *24*, 347−353. (d) Peruzzo, V.; Plazzogna, G.; Tagliavini, G. *Organomet. Chem.* **1972**, *40*, 129−133.

(32) Xiao, X.; Han, X.; Mei, Z.; Zhu, D.; Shao, K.; Liang, J. *J. Organomet. Chem.* **2013**, *729*, 28−39.

(33) Garbauskas, M. F.; Wengrovius, J. H. *Acta Crystallogr., Sect. C: Cryst. Struct. Commun.* **1991**, *47*, 1969−1971.

(34) Ramirez, A. R.; Parvez, M.; Ahmad, V. U.; Hussain, J.; Hussain, H. *Acta Crystallogr. Sect. E: Struct. Rep. Online* **2002**, *58*, m278−m280.

(35) Carraher, C. E., Jr. *Angew. Makromol. Chem.* **1973**, *31*, 115−122.

(36) Kittel, C. *Introduction to solid state physics*; Wiley: Hoboken, NJ, 2005.

(37) Gonze, X.; Lee, C. *Phys. Rev. B* **1997**, *55*, 10355−10368.

(38) Martin, R. M. *Electronic Structure: Basic Theory and Practical Methods*; Cambridge University Press: Cambridge, U.K., 2008.

(39) Dissado, L. A.; Fothergill, J. C. *Electrical Degradation and Breakdown in Polymers*; IET: London, 2006.

(40) Ceresoli, D.; Tosatti, E.; Scandolo, S.; Santoro, G.; Serra, S. *J. Chem. Phys.* **2004**, *121*, 6478−6484.

(41) Baldwin, A. F.; Ma, R.; Mannodi-Kanakkithodi, A.; Huan, T. D.; Wang, C.; Tefferi, M.; Marszalek, J. E.; Cakmak, M.; Cao, Y.; Ramprasad, R.; Sotzing, G. A. *Adv. Mater.* **2015**, *27* (2), 346−351.

DOI: 10.1021/ma502424r
Macromolecules XXXX, XXX, XXX−XXX